

## **Spatial Distribution of Gas Hydrate Deposits in Krishna-Godavari Offshore Basin, Bay of Bengal**

**C.K. Mishra<sup>1,2</sup>, P. Dewangan<sup>\*,1,2</sup>, G. Sriram<sup>1</sup>, A. Kumar<sup>1</sup>, Dakara. G.<sup>1</sup>**

<sup>1</sup>CSIR-National Institute of Oceanography, Dona Paula, Goa, India, 403004

<sup>2</sup>Academy of Scientific and Innovative Research (AcSIR), Ghaziabad- 201002, India

\* Corresponding author Email: [pdewangan@nio.org](mailto:pdewangan@nio.org)

### **Abstract**

To delineate the occurrences of gas hydrates and free gas in the Krishna-Godavari (KG) basin, Bay of Bengal, we used 3D seismic data to construct a velocity model of high spatial density. We used an automated version of migration velocity analysis to estimate P-wave velocities using Kirchhoff prestack time migration. We manually checked all common image gathers (CIGs) to assess the reliability of the auto-picking algorithm. The velocity model was validated against available down hole information from drilling Sites NGHP-01-02, NGHP-01-03, and NGHP-01-10. The model shows a) anomalously high velocities at Site NGHP-01-10 where significant gas hydrates were reported and b) background velocities at Sites NGHP-01-02 and NGHP-01-03 where a negligible amount of hydrate was recovered. A bottom simulating reflector (BSR) is identified in the 3D seismic data, and an average velocity map is prepared above the BSR. Background velocities of marine sediments in the KG basin vary from 1.43 km/s to 1.6 km/s; velocities higher than 1.65 km/s indicate gas hydrate bearing sediments while velocities lower than 1.43 km/s indicate free gas bearing sediments. High velocities observed below sea floor mounds and ridges suggest the presence of gas hydrate in a structurally deformed area. Slope basins are generally devoid of gas hydrates. Free gas is observed at depths of up to several hundred meters below the BSR suggesting the migration of deeper fluid/gas into the gas hydrate stability zone (GHSZ). Zones of gas hydrates and free gas are preferentially oriented along major faults indicating the role of faults in the transportation of free gas and formation of gas hydrate deposits. We identify a free gas bearing horizon at depths (> 300 m) below the BSR, which might contribute to the lateral migration of free gas. Gas hydrate deposits in KG basin are classified into two categories: i) leaky deposits which occur in the areas of active seafloor faults, and are characterized by heterogeneous distribution of gas hydrates, and ii) non-leaky deposits which are formed in areas of subsurface faults, and show a relatively homogeneous distribution of gas hydrates. Site NGHP-01-10 is an good example of leaky gas hydrate deposits above a deep-seated gas reservoir.

## 1. Introduction

Gas hydrates are crystalline solids which store methane or lighter hydrocarbon gases and are stable at high pressures and low temperatures (Sloan and Koh, 2007). Gas hydrates have received worldwide attention owing to their potential to store enormous volume of methane gas (Boswell and Collett, 2011), and several countries such as the USA, Japan, India, and China are developing technologies for the production of gas from hydrate deposits. Gas hydrates are also of key interest for climate studies as the stored methane is a greenhouse gas (Kvenvolden, 1988), and are also considered to represent a geohazard (Schmuck and Paull, 1993). The presence of gas hydrate/free gas is often inferred from the occurrence of an anomalous bottom simulating reflector (BSR) in seismic data, at a depth which usually coincides with the base of the gas hydrate stability zone (BGHSZ) (Shipley et al., 1979; Kvenvolden and McDonald, 1985; Singh et al., 1993). The BSR shows characteristic properties such as mimicking the seafloor, reversed (negative) polarity, and cross-cutting the geological reflectors. A BSR is manifested in seismic data due to the impedance contrast between gas hydrate-bearing sediments above and the free gas-bearing sediments below (Helgerud et al., 1999; Singh et al., 1993). However, drilling expeditions worldwide have shown that the BSR is not a reliable proxy for the mapping of gas hydrate deposits (Majumdar et al., 2016). A strong BSR can occur due to the presence of a small amount of free gas below the GHSZ without any significant amount of gas hydrates.

Therefore, there is a need for an alternate proxy for mapping large gas hydrate deposits. The acoustic velocity of shallow marine sediments can be used for mapping gas hydrate deposits as the presence of gas hydrates increases the P-wave velocity (Stoll et al., 1971). A number of studies have estimated P-wave velocities from multi-channel seismic (MCS) data, and used the results to infer the presence of gas hydrate deposits. The interval velocities derived from 2D MCS data established the presence of hydrate immediately above a BSR and free gas below it (Singh et al., 1993; Minshull et al., 1994). They attributed the upward migration of methane into GHSZ as a primary mechanism for hydrate formation. Yuan et al. (1996) and Tinivella and Accaino (2000) showed that velocities derived from MCS data can be used to estimate hydrate saturations using a suitable rock-physics model. Westbrook et al. (2008) showed that lateral variation in velocities is related to spatial distribution of hydrate and is controlled by migration pathways of free gas below the BSR. In clay-rich sediment, faults/fractures provide conducive pathways for gas migration and hydrate preferentially accumulates within faults/fractures in structurally deformed areas (Jaiswal et al., 2012). In addition, a permeable horizon may also provide pathways for gas migration (Crutchley et al., 2015). In some cases,

faults/permeable horizons may transport methane all the way up to seafloor causing methane seeps in the water column (Crutchley et al., 2010).

Expedition NGHP-01 was carried out for the exploration of gas hydrate deposits in the Krishna-Godavari basin, Bay of Bengal (Collett et al., 2008; Kumar et al., 2014). The occurrence of a BSR was used as a primary tool for the identification of drilling sites. Drilling confirmed the presence of fracture-filled gas hydrate deposits, and ~128 m thick massive hydrate was recovered from Site NGHP-01-10. Drilling also revealed considerable heterogeneity in the gas hydrate system as nearby Sites NGHP-01-12, NGHP-01-13 and NGHP-01-21 (within 500 m of NGHP-01-10) did not recover a hydrate deposit of such great thickness. This spatial variability was initially examined using a semblance-derived velocity model estimated from 2D seismic data (Dewangan et al., 2011). Later, the velocity model was refined using unified imaging (Jaiswal et al., 2012a) and full waveform inversion (Jaiswal et al., 2012b) which yielded fine-scale velocity variations, and showed structural and stratigraphic controls on the distribution of gas hydrate deposits in KG Basin. The distribution of gas hydrate in KG basin varies not only on this local scale but also on a regional scale as indicated by negligible recovery of gas hydrates at Sites NGHP-01-02 and NGHP-01-03, which are respectively located 1.36 km and 7.89 km from NGHP-01-10.

The objective of this study is to investigate the regional distribution of gas hydrate deposits and free gas, using velocities derived from an analysis of 3D seismic data covering an area of 153 km<sup>2</sup>. We use these data to map areas of gas hydrates and free gas bearing sediments and relate them to the distribution of surface and subsurface structures. The results allow us to examine the processes responsible for gas hydrate formation in relation to structurally-controlled upward fluid migration.

## **2. Geological setting of Krishna-Godavari Basin**

The Krishna-Godavari (KG) Basin is one of the most petroliferous basins on the eastern continental margin of India (Fig.1), which came into existence after the breakup of Gondwanaland around 130 Myr (Powell et al., 1988; Ramana et al., 1994; Scotese et al., 1988). The KG Basin covers an area of 28,000 km<sup>2</sup> onland and 145,000 km<sup>2</sup> offshore (Rao, 2001). The study area lies in the deep KG offshore in water depth between 700 and 1200 m (Fig. 1). Drilling Expedition NGHP-01 recovered significant amounts of fracture-filled gas hydrate deposits in the KG offshore basin (Collett et al., 2008; Kumar et al., 2014). Large scale structures in the KG offshore basin are primarily controlled by gravity-driven shale tectonism which occurs due to the movement of overpressured shale strata (Choudhuri et al., 2010; Dewangan et al., 2010). The major shale horizons in the KG offshore basin were rapidly deposited during Paleocene and

Eocene, and gas generation has led to overpressures within the formation (Rao and Mani, 1993; Singha and Chatterjee, 2014). Shale tectonism resulted in the development of toe-thrust faults and diapiric mounds in the offshore region (Dewangan et al., 2010).

A multibeam bathymetry map of the study area (Fig. 1; Ramana et al., 2009) includes NGHP-01 sites 02/03/10/12/13 (Kumar et al., 2014). The map shows several tongue-like features (e.g., MTD-1, MTD-4) which have been attributed to mass transport deposits (MTDs) in the slope basin (Dewangan et al., 2010; Mandal et al., 2014; Ramprasad et al., 2011). The movement of shale strata in the continental slope region has resulted in a series of toe-thrust faults (Choudhuri et al., 2010; Ramana et al., 2014) which are identified in multibeam bathymetry data as sedimentary ridges (Fig. 1). In addition, the movement of upper Miocene-Pliocene mobile shale strata formed shale bulges which are identified at seafloor as mounds (M1 and M2, Fig. 1). Bathymetric mounds (M1 to M4) and sedimentary ridges (SR1 and SR2) are considered to be the surficial expression of shale tectonism (Dewangan et al., 2010). These structures are associated with deep-rooted faults (Riedel et al., 2010) which provide a conducive environment for the movement of fluid/gas. Two fault groups (A and B) are observed in the study area; Group-A faults are predominantly oriented in the north-south direction while group-B faults are oriented in the east-west direction (Riedel et al., 2010). Fluids rich in methane form massive, fracture-filled gas hydrate deposits upon entering the gas hydrate stability zone (GHSZ). Some faults may transport methane up to the seafloor leading to a proliferation of chemosynthetic communities in KG Basin (Mazumdar et al., 2019). Geochemical and magnetic proxies along with fossil records of chemosynthetic communities show paleo-methane expulsion events from the mounds and toe-thrust regions of KG Basin (Mazumdar et al., 2009; Dewangan et al., 2013; Usapkar et al., 2014).

### **3. Data and Methodology**

The study uses 3D seismic data in the KG offshore basin covering Sites NGHP-01-02, NGHP-01-03, and NGHP-01-10 to delineate the occurrences of gas hydrated eposits (Fig. 1). The data were acquired by the Oil and Natural Gas Commission Ltd. (ONGC) onboard M/V Western Monarch in 2002. A dual air gun cluster of 2750 cu. in. was used as a seismic source and five 5 km long hydrophone cables with 200 channels were used as a receiver. The cables were separated from each other by 200 m. The shot interval was 50 m, and the receiver group interval was 25 m which translates in to a 60-fold common depth point (CDP) gather (Mandal et al., 2014). For the present study, we took a subset of the 3D data from two blocks across Sites NGHP-01-10 (NGHP10 block) and NGHP-01-03 (NGHP03 block), and reprocessed them independently of each other. Prestack 3D seismic data were loaded into ProMAX software, and geometry was assigned based on navigation

files. Data were binned into CDP gathers having an interval of 12.5 m along inline direction and 50 m along cross line direction. The record length of seismic data is 8 s and the dominant frequency is ~30 Hz. Vertical resolution, defined as one-fourth of wave length, is ~13 m assuming a velocity of 1600 m/s. Lateral resolution, defined by radius of the first Fresnel zone (Sheriff, 1980), is ~185 m at a depth of 1.3 km before migration and ~53 m after migration. The NGHP10 block covers an area of ~58 km<sup>2</sup> with 92 inlines and 1000 cross lines while the NGHP03 block covers an area of ~95 km<sup>2</sup> with 152 inlines and 1000 crosslines.

The initial velocity model was obtained for a grid of 500x500 m using a conventional semblance approach (Neidell and Taner, 1971). However, the velocity information was not useful for interpretation as it depends on the dip of reflector. Therefore, we adopted an established migration velocity analysis (MVA) technique (Biondi and Symes, 2004; Sava and Biondi, 2004; Stork, 1992; Yilmaz, 2001) to build the velocity model. MVA approach uses the flatness of common image gather (CIG) to estimate the velocity model. If migration velocities are close to true velocities, the reflectors in a CIG are flat, whereas incorrect velocities lead to under or over migration (Sava and Biondi, 2004; Yilmaz, 2001). Kirchhoff prestack time migrated images were obtained for a range of migration velocities, and the velocity that flattened the CIG for a particular horizon was assumed to be correct. In order to obtain the velocity model at each CIG, extensive manual picking is required which is time-consuming and laborious. Therefore, we adopted the auto-picking methodology proposed by Toldi (1989), in which auto-picking is guided along pre-defined horizons. Migration velocities were assumed to be the root-mean-square (RMS) velocities, and interval velocities between the layers were calculated from Dix's equation (Dix, 1955). The error in the interval velocity is inversely proportional to layer thickness (Hajnal and Sereda, 1981). Therefore, we picked horizons which are well-separated in time. The derived interval velocity model is interpreted to demarcate regions of gas hydrate (high velocity anomaly) and free gas (low velocity anomaly). The final velocity model is also used to generate prestack time-migrated images.

Migrated 3D seismic data were loaded into OpendTect software for seismic interpretation. We picked the seafloor manually for all in lines and crosslines and constructed a grid for the study area at a resolution of 12.5 m x 50 m. The grid was plotted using generic mapping tools (GMT) as a seafloor map. Numerous faults were observed on the seafloor map; therefore, a similarity map of the seafloor was prepared using the coherency analysis of adjacent seismic traces (De Rooij and Tingdahl, 2002) to better delineate the faults. In general, the homogeneous background sediments show similarity close to unity while the seafloor disturbed by faults / fracture network or any other laterally

heterogeneous features shows a low similarity. We picked the faults and categorized them into two groups A and B similar to those defined by Riedel et al. (2010).

We identified the BSR in the seismic data based on its characteristic properties and picked it manually wherever it was observed. Assuming that the BGHSZ coincides with depth of the BSR, an empirical relationship between depths of the BGHSZ and seafloor was established. The relationship was used for computing a BGHSZ grid from seafloor grid. Likewise, other prominent horizons were picked on seismic data and respective grids were constructed. The interval velocities were extracted at these horizons to construct the velocity maps.

## **4. Results**

### **4.1 Fault / fracture network from a seismically derived seafloor map**

A seafloor bathymetric map interpreted from the 3D seismic data (Fig.2a) shows mass transport deposits (MTD-1 and MTD-4), mounds (M1 and M2), and several lineations interpreted as surficial expressions faults. In the vicinity of Site NGHP-01-10, we observe the most extensive fault/fracture system dominated by Group-A faults. A prominent fault oriented in NNW-SSE direction (marked as A) is observed with several small scale faults oriented in the NE-SW direction (Fig. 2c). A similar fault system is observed in the western part, however, the fault/fracture system is not observed near Site NGHP-01-03.

### **4.2 Seismic velocities for selected profiles**

Interval velocities estimated using the automated version of MVA are shown along selected 3D seismic in lines in Fig. 3 (locations in Fig. 2c). Seismic profile IN-A crosses Site NGHP-01-03 in the slope basin (Fig. 3a). Reflectors corresponding to the seafloor, BSR, and a deeper gas horizon are marked on the section as well as on the velocity model. Several faults are also marked which correlate well with the seafloor map. A weak BSR is observed ~250ms TWT (two way travel time) below the seafloor from CDPs 2000 to 2200 and from 2600 to 2800. The interval velocity of the profile increases from 1.5 km/s at the seafloor to ~1.7 km/s at 600 ms below the seafloor (Fig. 3a). A few high velocity anomalies are observed above the BSR. In general, no drop in interval velocity is observed below the BSR, however, a low-velocity patch is observed across a group-B fault. No velocity anomaly is observed at Site NGHP-01-03.

Seismic profile IN-B (Fig. 3b) also lies in the slope basin and transects mass transport deposits (MTD-4) observed on the seafloor map (Fig. 2a). Towards the southern end of the line, the profile crosses a major group-B fault. A BSR is clearly identified from CDPs 2500 to 2800 and is patchy within the slope basin. Some high velocity anomalies (>1.7 km/s) are observed above the BSR from

CDPs 2000-2100 and 2700-2800 and velocities drops to  $<1.3$  km/s below the BSR. Low velocities (1.2-1.3 km/s) are also observed across MTD-4 from CDPs 2350 to 2650.

Seismic profile IN-C (Fig. 3c) transects all the major fault groups, and crosses the heavily faulted seafloor mound M1 towards the southern end near Site NGHP-01-10. A BSR is observed across the section at  $\sim 200$ -250 ms below the seafloor. Anomalously high-velocities are observed above BSR between CDPs 2080 and 2160 near Site NGHP-01-10 where the velocity increases from  $\sim 1.6$  km/s to  $>2$  km/s. Drilling results through these patches indicate the presence of fracture-filled gas hydrate deposits (Kumar et al., 2014). Other high-velocity anomalies are observed between CDPs 1500-1700 and CDPs 1750-1850 around a group-B fault. Anomalously low velocity values of  $\sim 1.2$  km/s are observed below the BSR between CDPs 2080-2160 and the low velocities extend to deeper horizons at up to 2 s TWT. A high amplitude, low-frequency horizon is observed below the BSR which will be referred to as a gas bearing horizon. The seismic reflection amplitudes from the geological layers below this horizon are significantly reduced due to attenuation.

Seismic profile IN-D (Fig. 3d) crosses the western part of mound M1 and near Site NGHP-01-02. A high amplitude but patchy BSR is observed along this profile, but is difficult to identify beyond CDP 2180 as it merges with a deeper gas horizon. Isolated high velocity anomalies are observed above the BSR between CDPs 1550-1650, 1980-2050 and 2200-2400 where the BSR merges with the gas horizons. No velocity anomaly is observed at Site NGHP-01-02, where the log data show a negligible amount of gas hydrate (Kumar et al., 2014). A high amplitude and low-frequency gas horizon is also observed in this profile below the BSR, and the seismic reflection amplitudes from deeper horizons are significantly reduced. The interval velocity model complements the seismic section, and low velocities ( $<1.3$  km/s) are observed below the gas horizon from CDPs 2000 to 2250. Similar low velocities are also observed up to 50 ms below the seafloor between CDPs 1550 and 2100.

Seismic profile IN-E (Fig. 3e) lies in the western part of the study area and transects bathymetric mound M2 which is heavily faulted. A BSR is observed in the seismic section  $\sim 200$ -250 ms below the seafloor, although its identification is difficult beyond CDP 2200. A continuous high-velocity anomaly is observed above the BSR from CDPs 1600 to 2100 where the velocity increases from  $\sim 1.6$  km/s to  $\sim 1.75$  km/s. In the southern end of the profile, a similar high-velocity anomaly is observed from CDPs 2200 to 2400 where the velocity is  $>1.75$  km/s. No velocity anomaly is observed immediately below the BSR. A high amplitude and low-frequency gas horizon is also observed in this profile and low velocities ( $<1.3$  km/s) are observed below the gas horizon from CDPs 1600 to 2350. The reflection amplitudes from deeper horizons are reduced. A high amplitude horizon with a

polarity similar to the seafloor is observed 70-100 ms TWT below the seafloor and matches well with the top of the high-velocity zone.

#### **4.3 Reliability of auto-picking algorithm in estimating seismic velocity**

We performed a quality check on the auto-picking algorithm to assess its reliability in estimating seismic velocity. Semblance plots were generated to measure the flatness of common image gathers (CIGs) as a function of migration velocities and two-way traveltimes (TWT). Fig. 4a presents the semblance plot for seismic profile IN-A at CIG 2566 near Site NGHP-01-03 and shows a monotonous increase in velocity with depth. No high or low-velocity anomaly is observed across the BSR, and results from Site NGHP-01-03 confirm that it contains negligible amount of gas hydrate (Kumar et al., 2014). Therefore, the velocity profile in Fig. 4a represents the background velocity profile in the study area. Fig. 4b presents the semblance plot for profile IN-B at CIG 2051 where a BSR is observed at ~1.6 s TWT. An increase in velocity is observed from 1.4 s TWT down to the BSR and a drop in velocity is observed below the BSR down to 1.8 s TWT. Fig. 4c presents the semblance plot for profile IN-C at CIG 2128 near Site NGHP-01-10 where a BSR is observed at ~1.58 s TWT. A significant increase in velocity is observed from 1.5 s TWT down to the BSR and a minor drop in velocity is observed below the BSR down to 1.75 s TWT. Results from Site NGHP-01-10 show ~128 m of fracture-filled gas hydrate deposit above the BSR (Kumar et al., 2014). The semblance plot shows a significant drop in velocity below 1.9 s TWT indicating a wide spread low-velocity anomaly beneath Site NGHP-01-10. Fig. 4d presents the semblance plot for profile IN-D at CIG 2096 near Site NGHP-01-02 where a BSR is observed at ~1.61 s TWT. The velocities are similar to background above the BSR while significantly lower velocities are observed below the BSR down to 1.9 s TWT. Log data from NGHP-01-02 indicate an negligible amount of hydrate despite a well-developed BSR (Kumar et al., 2014). Fig. 4e presents the semblance plot for profile IN-E at CIG 1825 where a BSR is observed at ~1.62 s TWT. Increased and decreased in velocities are observed above and below the BSR, respectively. Fig. 4f presents the semblance plot for profile IN-E at CIG 2327 where a similar increase and decrease in velocities is observed above and below the BSR (~1.88 s TWT). Overall, the velocities auto-picked by the algorithm follow the maximum semblance values. Further, the inferences deduced from the velocity trends match well with the results from NGHP-01. Therefore, the velocities picked from the algorithm are considered to be reliable.

#### **4.4 Comparison between the seismic derived velocities and velocities obtained from sonic logs**

The sonic velocities of Sites NGHP-01-02, NGHP-01-03, and NGHP-01-10 are converted from depth to TWT below seafloor and compared with the seismic derived interval velocities (Fig. 5a). Sites NGHP-01-02 and NGHP-01-03 represent the background velocity trend in both logging



and seismic-derived velocities, which vary from ~1.45 km/s near the seafloor to ~1.6 km/s at 300 ms TWT below the seafloor. P-wave velocities ( $V_p$ ) greater than 1.7 km/s indicate the presence of hydrates and less than 1.4 km/s indicate free gas (Jaiswal et al., 2012a). Interval velocities at Site NGHP-01-10 are up to ~1.85 km/s from 100 to 160 ms TWT and drop to <1.3 km/s below the BSR. A high-velocity zone in the shallow part of the sonic data from Site NGHP-01-10 is not observed in the seismically derived velocities and maybe a local anomaly beyond the lateral resolution of the seismic data. The BSR marks the transition from high velocity (hydrate) to low velocity (possibly free gas). The mean and standard deviation of the velocities are obtained by averaging the nearby CIGs, and shows a 99% confidence level in the velocities. A cross plot between the sonic velocities and the interval velocities is shown in Figure 5b for different Sites NGHP-01-02, 03, and 10. Velocities for Sites NGHP-01-02 and NGHP-01-03 represent background values for marine sediments, whereas high velocities at Site NGHP-01-10 show the presence of gas hydrates. The log-derived velocities of marine sediments vary from 1.43 km/s at the seafloor to 1.6 km/s at BSR depth. Therefore, we assume a velocity range of 1.43 to 1.65 km/s for the background sediments and an average velocity of 1.6 km/s at BSR depth. Jaiswal et al. (2012a) assumed velocities larger than 1.7 km/s to be a firm indicator of gas hydrate and velocities smaller than 1.4 km/s to be a firm indicator of free gas while Dewangan et al. (2011) assumed 1.6 km/s to be the average velocity of background marine sediments. The effective medium model (EMM) yielded similar background velocities for Site NGHP-01-03 (Sriram et al., 2014).

#### **4.5 Seismically derived interval velocity map above the BGHSZ**

We delineate occurrences of gas hydrates by constructing a map of interval velocities above the BGHSZ (Fig. 6). Interval velocities were extracted over an interval of 80 ms above the BGHSZ and averaged to minimize the effect of vertical heterogeneity. Averaging yielded a consistent velocity model used to map zones of anomalously high or low velocities. We manually checked the accuracy of the auto-picking algorithm for all CIGs and identified areas where the semblance plot was not reliable due to poor data quality. Those areas were not taken into account in preparing the velocity maps. In addition, we removed unrealistic velocity values using the concept of outliers (Thompson, 1985) within a radius defined by the Fresnel zone. The average interval velocity map above the BGHSZ is shown in Figure 6. High-velocity anomalies are observed beneath the mounds and across sedimentary ridges. Velocities vary from ~1.55 km/s to ~1.65 km/s in the slope basin area and increase to more than 1.70 km/s beneath mounds M1 and M2 and to more than 1.75 km/s in the southern part of the study area across these sedimentary ridge

SR1. Velocities  $>1.65$  km/s are attributed to gas hydrate deposits. The interpreted areas of gas hydrates are classified into four zones (Zones I to IV). Zones I and III correspond to gas hydrate deposits in areas of high-density faulting. Within Zone I, results from Site NGHP-01-10 confirm the presence of fracture-filled gas hydrate (Kumar et al., 2014). Zone II represents gas hydrate deposits in areas relatively low-density faulting. Zone IV also corresponds to an area of enhanced velocities ( $>1.7$  km/s) which may be associated with extensive gas hydrate deposits.

#### **4.6 Seismically derived interval velocity map below the BGHSZ**

Next, we delineate occurrences of free gas by constructing an interval velocity map below the BGHSZ. The velocity map is prepared by averaging the velocities over an interval of 80 ms below the BGHSZ (Fig. 7a). The map shows an average velocity of 1.65 km/s in the slope basin, decreasing to less than 1.45 km/s in Zones I and III. Interestingly, the map shows slow-velocity anomalies in the same areas where high-velocity anomalies are observed above the BGHSZ. In Zones I and III, areas of high-density faulting, low-velocity anomalies appear to be oriented along the trend of the major fault groups. We observe a minor drop in velocity ( $<1.55$  km/s) in Zone II, a region of low-density faulting. In zone IV, we observe low velocities ( $<1.55$  km/s) below the BGHSZ. Velocities lower than the average background ( $<1.6$  km/s) may indicate the presence of free gas while velocities lower than 1.43 km/s are a good indicator of free gas. At Site NGHP-01-03, we observe a low velocity anomaly indicating the migration of free gas through the fault system. The velocity model along selected profiles (Fig. 3) shows the presence of a deeper gas horizon which may act as a conduit for the lateral migration of free gas into the GHSZ.

We prepared average velocity maps above this horizon (Fig. 7b) and below it (Fig. 7c) to understand the deep plumbing system in the KG offshore basin. In Zone I, a significant drop in velocities ( $< 1.43$  km/s) above and below the horizon shows the presence of free gas. Zones II and III show similar low-velocities confirming that deep-seated gas reservoirs are feeding gas through the fault system to form gas hydrates within the GHSZ. The velocity map at a constant TWT of 2s (Fig. 7d) shows a prominent zone of gas located below the area of high-density faulting around Site NGHP-01-10. A similar conclusion was drawn by Riedel et al. (2010) based on the attribute analysis of 3D seismic data.

#### **4.7 Gas hydrate saturation map from seismic velocities**

Gas hydrate saturation can be estimated from seismic P-wave velocities using a variety of rock physics models that depend on the distribution of gas hydrate within these sediments (Helgerud et

al.,1999; Sriram et al.,2014). In the present study, we adopted the grain-to-grain contact effective medium theory (EMT) of Sriram et al. (2014) to estimate gas hydrate saturation from the average interval velocity above the BGHSZ. The background P–wave velocity is estimated to be 1.57 km/s at BSR depth using the physical properties of Site NGHP-01-03 (Table 1; Sriram et al., 2014) assuming ~95 % clay and ~5 % quartz with an average porosity of ~53 % and an average grain contact of five. The difference between the background velocity and the average interval velocities is expressed in terms of gas hydrate saturations using the EMT (Fig. 8). Gas hydrate saturations vary from 10-20 % in Zones I–III to greater than 30% in zone IV. The gas hydrate saturation (~20 %) at Site NGHP-01-10 matches well the saturation reported from pressure cores (Kumar et al., 2014). In Zones I and III, the gas hydrate distribution is patchy and mostly controlled by the fault system, whereas the distribution is relatively homogeneous in Zone II.

## **5. Discussion**

### **5.1 Structural control on the formation of gas hydrate deposits**

The formation and distribution of gas hydrate deposits are often structurally and stratigraphically controlled by fluid migration along permeable pathways (Milkov and Sassen, 2002). In structural accumulations, gases are transported to the GHSZ through faults and fracture systems, e.g. northwestern Gulf of Mexico (Brooks et al., 1986; Milkov and Sassen, 2002, 2001; Sassen et al., 2001) and Hydrate Ridge (Hovland et al., 1997; Suess et al., 2001; Torres et al., 2004). In the KG Basin, the mounds and ridges are associated with deep-rooted fault systems, and some of the faults are still active as evident from their seafloor expression (Figs. 2b,d). Our results confirm that these faults act as conduits for the passage of fluid/gas from deep-seated reservoirs to the shallow subsurface. The average interval velocity map above the BGHSZ (Fig. 6) shows gas hydrate zones (I–IV) beneath the mounds and toe-thrust ridges. Drilling results in Zone I confirm the presence of massive, fracture-filled gas hydrate deposits at Site NGHP-01-10 (Kumar et al., 2014). In contrast, the interval velocity map indicates a negligible amount of gas hydrates in the slope basin, consistent with drilling results from Site NGHP-01-03. Therefore, areas of structural deformation due to shale tectonism are favorable locations for the formation of gas hydrate deposits within the KG Basin. We infer the fault/fracture systems to provide pathway for the upward migration of fluid/gas which, upon entering the gas hydrate stability zone, form gas hydrate deposits. The precipitation of gas hydrate in marine sediments may also lead to the formation of secondary fractures which enhance primary pathways provided by the fractures. However, we infer that the permeable pathways provided by fault/fracture systems are critical for the formation and distribution of gas hydrate deposit in clay-rich sediments.

Structural and tectonic settings similar to the KG Basin are found in other active and passive continental margins associated with gas hydrate deposits. The Kumano Basin, offshore SE Japan, is part of the Nankai accretionary system and contains widespread gas hydrate deposits (Kinoshita et al., 2011; Bale et al., 2014). The Nankai Trough is filled with thick turbidites, in contrast to the clay-dominated KG basin. However, the compressional tectonics of the Nankai system also create fault-fracture systems that provide pathways for deep-seated fluids to migrate in the GHSZ and form gas hydrate accumulations. The northern part of the South China Sea off SW Taiwan is an accretionary margin associated with multiple thrust faulting and widespread occurrence of gas hydrate deposits (Berndt et al., 2019). The Hikurangi margin located off the east coast of New Zealand is another example of active margin with gas hydrate deposits, in which major thrust fault systems provide pathways for the upward migration of deep-seated gas-charged fluids (Crutchley et al., 2010, 2015). Analysis of 3D seismic data from the Nankai Trough accretionary prism suggests that focused fluid migration through major faults leads to higher heat flow, and is a likely mechanism for the formation of gas hydrate deposits (Bale et al., 2014). Analysis of 3D seismic data in the KG Basin suggests that the BSR-derived geothermal gradient increases by 10-15 % across major fault system due to focused fluid flow in Zones I and III (Mandal et al., 2014). These findings are consistent with our proposal that the likely mechanism for the formation of gas hydrate deposit within the KG basin is focused fluid flow through major fault system.

## **5.2 Migration of deep-seated free gas along permeable pathways**

Methane gas which forms the hydrate deposit is transported through diffusion or advection or both processes from deeper regions. In the KG offshore basin, a prominent high amplitude horizon is observed below the BSR. Maps of average interval velocity above (Fig. 7b) and below this horizon (Fig. 7c) show a low-velocity anomaly within Zones I-III indicating the presence of deep-seated free gas. Therefore, it is likely that this horizon forms part of a permeable pathway for the upward migration of deep-seated fluid/gas. A velocity map prepared at a constant time of 2 sTWT (Fig. 7d) confirms that Zone I, which hosts Site NGHP-01-10, overlies a deep-seated gas reservoir. We therefore propose that gas from deeper sources enters the GHSZ primarily through faults/fractures by advection, and forms large scale fracture-filled gas hydrate deposits in Zones I-III.

Several possible factors in KG Basin can produce a significant quantity of methane gas. Analysis of regional seismic lines in the Bay of Bengal indicates high sedimentation rates due to the growth and erosion of the Himalayas during the past 800 kyr (Krishna et al., 2016). High discharge of the Krishna and Godavari rivers coupled with a narrow shelf of the KG Basin led to rapid deposition of upper slope sediments. Organic matter is well preserved due to high sedimentation rates and produces methane upon burial (Canfield, 1994). Geochemical analyses of gas recovered from Sites

NGHP-01-10, NGHP-01-12, and NGHP-01-13 suggest that biogenic methane is dominant (Kumar et al., 2014; Peketi et al., 2012). Methane forms shallow hydrate under suitable temperature and pressure conditions, which may dissociate upon burial and release significant amount of methane to form deep-seated gas reservoirs (Kundu et al., 2008). Fluid/Gas migrates along the regional fault/fracture system from deep-seated gas reservoir yielding large scale gas hydrate deposits in the KG Basin.

### **5.3 Leaky vs. Non-leaky gas hydrate deposits**

The inferred distribution of gas hydrate within Zones I and III differs from Zone II despite the similarity in the geological structures. In Zones I and III, gas hydrate is preferentially distributed along the fault/fracture network and shows strong heterogeneity. In Zone I, results from multiple drilling Sites (NGHP-01-10, 12, and 13) separated by short distances revealed marked differences in gas hydrate saturation (Kumar et al., 2014). Site NGHP-01-10 showed a thick hydrate deposit extending from 30 m below the seafloor to the depth of BSR, whereas nearby Sites NGHP-01-12 and 13 showed limited gas hydrate deposits above the BSR. Low-velocity anomalies are observed along some faults suggesting the migration of free gas within the GHSZ (Fig. 6). The velocity model obtained using full waveform inversion around Site NGHP-01-10 also shows low velocities along a fault (Jaiswal et al., 2012b). Further, the attenuation model shows strong attenuation along the same fault confirming the presence of free gas (Dewangan et al., 2014). Giant piston cores recovered by the *Marion Dufresne* have confirmed the paleo-migration of free gas around 46.2 - 53.0 kyr, and the migration of gas to seafloor is recorded by a proliferation of chemosynthetic communities at Site NGHP-01-10 (Collett et al., 2008; Mazumdar et al., 2009). In contrast, gas hydrate deposits are more homogenous in zone II with fewer occurrences of free gas-bearing sediments. The bathymetry and seafloor similarity map also show Zones I and III to differ from Zone II. Faults extend to the seafloor in Zones I and III indicating recent activity, whereas the surficial expression of faults is not observed in Zone II.

We suggest that the distribution of gas hydrate deposits in the KG Basin can be classified into two categories: leaky gas hydrate deposits and non-leaky deposits. Zones I and III correspond to leaky deposits where the fault system is active and expressed as deformation of the seafloor. The active fault system facilitates the upward migration of fluid/gas, which in places can escape the seafloor and discharge into the water column as gas flares (Gullapalli et al., 2019). The occurrence of free gas within the GHSZ leads to an intricate pattern of gas hydrate and free gas bearing zones which is reflected in the velocity model as high and low-velocity zones. Therefore, leaky gas hydrate deposits show strong lateral heterogeneity. In contrast, Zone II belongs to non-leaky gas hydrate deposit

where faults are restricted to the subsurface. The high-velocity zone representing gas hydrate deposits occurs as a relatively homogeneous layer with a negligible presence of free gas-bearing sediments. In contrast to leaky gas hydrate deposit, the non-leaky deposit has more potential to store a large amount of gas hydrate deposit. A conceptual model explaining the salient features of leaky vs non-leaky gas hydrate deposit is shown in Figure 9.

Finally, we consider how free gas and hydrate can co-exist in the GHSZ. Site NGHP-01-10 provides evidence of shallow gas hydrate deposits occurring 30 m below seafloor(Kumar et al., 2014) and coreMD161/8 contained geological/geochemical signatures of paleo-methane venting events (Mazumdar et al., 2009). Several mechanisms can explain high methane flux near the seafloor. For example, analysis of seismic data from the Hikurangi margin, New Zealand(Pecher et al., 2010) and the Nankai accretionary prism, SE Japan (Bale et al., 2014) suggests that the base of GHSZ may be locally upwarped due to focused fluid flow. Alternatively, upwarping of the BGHSZ may be caused by perturbation of salinity, temperature and pressure conditions and permeability of the host sediment due to hydrate formation (Liu and Flemings, 2007). The formation of gas hydrate within fault systems increases the salinity of surrounding pore water to the extent that the stability zone is perturbed, leading to free gas migration within the GHSZ. An additional mechanism for explaining free gas migration within GHSZ is the increase in overpressure due to the presence of free gas or the generation of secondary fractures due to hydrate formation, resulting in nonlinear methane flux rates to the seafloor(Stranne et al., 2017).In order to resolve which mechanism is responsible for the migration of free gas through GHSZ in the KG offshore basin, additional geological/geophysical/geochemical investigations are warranted.

## **6. Conclusions**

A velocity model of high spatial density derived from 3D seismic data is used to map the distribution of gas hydrate-bearing and free gas-bearing sediments in the Krishna-Godavari Basin, Bay of Bengal. Areas of anomalously high velocity within the GHSZ are interpreted to record the presence of gas hydrate, while low-velocity anomalies below the BSR are interpreted to result from free gas. Velocities derived from seismic data match well with those obtained from sonic logs. The main findings can be summarized as follows:

- i) The spatial distribution of gas hydrates is structurally controlled in the KG basin, and bathymetric mounds formed due to shale tectonics are favorable locations for the formation of gas hydrate deposits.

- ii) Free gas-bearing sediments are observed below the BGHSZ in areas of gas hydrate, suggesting the presence of deep-seated gas reservoirs.
- iii) Velocity anomalies indicative of gas hydrates and free gas are oriented along the major fault systems indicating that tectonic structures are critical to provide permeable pathways for gas migration in clay-dominated sediments.
- iv) Gas hydrate deposits can be classified into two categories: a) zones of active faults show leaky gas hydrate deposits characterized by a heterogeneous distribution of hydrate and free gas, b) zones of inactive faults show non-leaky deposits with a relatively homogeneous distribution, which have the potential to store large volumes of gas hydrates.

### **Acknowledgments**

We thank the Director, CSIR-National Institute of Oceanography (NIO) for supporting the gas hydrate program at CSIR-NIO. We also extend our sincere thanks to the Director General, Directorate General of Hydrocarbons (DGH) and Oil and Natural Gas Commission (ONGC) for providing valuable 3D seismic data for the present study. The technical committee members of National Gas Hydrate Programme (NGHP) especially K.K. Chopra (DGH) and S. K. Roy (DGH) are gratefully acknowledged for their comments and suggestions. We also acknowledge the CSIR project MLP1601 which supported the development of software codes for velocity analysis. We acknowledge Sushmita Kadam and Satyendra Panwar for providing support in the development of the code for velocity analysis. We thank K. Sudheesh for providing the slot in the Linux cluster for running the velocity analysis code. We thank two anonymous reviewers, Tiago M. Alves and associate editor Daniel Praeg for providing comments and suggestions which have improved the quality of the manuscript. C.K. Mishra would like to thank the CSIR for providing financial support through an award of SRF fellowship. The work was performed under CSIR-GEOSCAPE and MLP 1601 programs, and the CSIR-NIO contribution no is xxxx.

## Figure Captions

**Figure 1.** High-resolution bathymetry map of the study area in the Krishna-Godavari offshore basin, Bay of Bengal (modified after Dewangan et al., 2010). The inset shows the location of the KG Basin with respect to the Indian subcontinent. The dashed box shows 3D seismic data used in the present study, obtained from two blocks: NGHP10 and NGHP03. Bathymetric features such as mounds (M1-M4), sedimentary ridges (SR1 and SR2), channels and delta fronts are marked on the map. Sites drilled during NGHP-01 (marked as KG) are shown by stars. Sites NGHP-01-02 (KG-02), NGHP-01-03, and NGHP-01-10 lie within the area demarcated by 3D seismic data. Core MD161/8 lies near Site NGHP-01-10.

**Figure 2.** a) 3D seismic-derived seafloor bathymetry across Sites NGHP-01-02, NGHP-01-03, and NGHP-01-10; b) similarity map derived from coherency analysis of seismic data; c) interpreted seafloor map; d) faults picked on seafloor similarity map; two distinct fault groups (A and B) are observed in the study area. The lines (IN-A to IN-E) show the seismic profiles used in the present study.

**Figure 3.** Prestack time migrated 3D seismic inline (top) and estimated interval velocities (bottom) for five seismic profiles (IN-A to IN-E), locations shown in Figure 2c and 2d. Seismic profiles IN-A to IN-E and their corresponding velocity models are shown in panels (a)-(e), respectively. Reflectors corresponding to the seafloor, a bottom simulating reflector (BSR), and a deeper gas horizon are marked on the seismic profiles. Several faults are also marked on the profiles which correlate with those on the seafloor map (Fig. 2d). The throw across the faults is indicated using half-arrows. Solid ellipses represent high velocity anomalies and dashed ellipses low velocity anomalies.

**Figure 4.** Semblance plots for CIGs selected from seismic profiles (IN-A to IN-E) illustrating the reliability of the auto-picking algorithm. Stars show the velocities picked by the algorithm. In general, the velocities follow the local maxima in the semblance plot. Dotted lines mark the locations of the BSR in seismic data. In general, high-velocity anomalies (solid bars) above the BSR indicate the presence of gas hydrate while low velocity anomalies (hatched bars) below the BSR indicate the presence of free gas.

**Figure 5.** Comparison between velocities derived from sonic logs vs seismic intervals for drilling Sites NGHP-01-02, NGHP-01-03, and NGHP-01-10. At Site NGHP-01-10, high and low velocity anomalies are observed above and below the BSR, respectively. In contrast, Sites NGHP-01-02 and NGHP-01-03 are devoid of high or low-velocity anomalies and are considered to represent the background marine sediments. Velocities higher than 1.65 km/s are interpreted to indicate the presence of gas hydrates while velocities lower than 1.43 km/s indicate free gas.

**Figure 6.** Average velocity map (averaged over 80 ms TWT) above the BSR illustrating velocity variations that can be related to the spatial distribution of gas hydrate deposits in the 3D seismic study area. The high-velocity anomalies are observed beneath bathymetry mounds (M1 and M2) and sedimentary ridges. The lines represent the surficial expression of faults interpreted from the seafloor similarity map. The areas of high-velocity anomalies have been divided into four different zones (Zones I to IV).

**Figure 7.** a) Average velocity map (averaged over 40 ms TWT) below the BSR in the study area; b) Average velocity map above the gas horizon; c) Average velocity map below the gas horizon; d) Velocity map at a constant time slice of 2 s TWT. The low-velocity anomalies represent the occurrence of the free gas-bearing sediments.

**Figure 8.** Gas hydrate saturation map in the study area. The map is derived from the average interval velocity using the rock physics model of Sriram et al. (2014).

**Figure 9.** Salient features of leaky (a) and non-leaky (b) gas hydrate deposits. In leaky deposits, faults extend up to the seafloor and methane can be transported from deeper regions to the seafloor. The spatial distribution of hydrates is laterally heterogeneous, and deep-seated gas reservoirs are observed below such deposits. In contrast, the distribution is relatively homogeneous for non-leaky deposits. Faults are mostly limited to subsurface and the occurrences of methane seeps are rare. A permeable horizon may also contribute towards upward migration of methane.



## References

- Bale, S., Alves, T. M., Moore, G. F., 2014. Distribution of gas hydrates on continental margins by means of a mathematical envelope: A method applied to the interpretation of 3D Seismic Data. *Geochemistry, Geophys. Geosystems*, 15(1), 52-68.
- Biondi, B., Symes, W.W., 2004. Angle-domain common-image gathers for migration velocity analysis by wavefield-continuation imaging. *Geophysics* 69, 1283–1298.
- Berndt, C., Chi, W.C., Jegen, M., Lebas, E., Crutchley, G., Muff, S., Hölz, S., Sommer, M., Lin, S., Liu, C.S., Lin, A.T., 2019. Tectonic Controls on Gas Hydrate Distribution Off SW Taiwan. *J. Geophys. Res. Solid Earth*, 124(2), 1164-1184.
- Brooks, J.M., Cox, H.B., Bryant, W.R., Kennicutt, M.C., Mann, R.G., McDonald, T.J., 1986. Association of gas hydrates and oil seepage in the Gulf of Mexico. *Org. Geochem.* 10, 221–234.
- Choudhuri, M., Guha, D., Dutta, A., Sinha, S., Sinha, N., 2010. Spatiotemporal variations and kinematics of shale mobility in the K-G Basin, India. In: Wood, L. (Ed.), *Shale Tectonics*, AAPG Memoir, vol. 93, 91-109.
- Collett, T.S., et al., 2008. Results of the Indian National Gas Hydrate Program Expedition 01 Initial Reports, Report. Director General of Hydrocarbons, Ministry of Petroleum and Natural Gas, New Delhi.
- Crutchley, G. J., Pecher, I. A., Gorman, A. R., Henrys, S. A., Greinert, J., 2010. Seismic imaging of gas conduits beneath seafloor seep sites in a shallow marine gas hydrate province, Hikurangi Margin, New Zealand. *Marine Geology*, 272(1-4), 114-126.
- Crutchley, G.J., Maslen, G., Pecher, I.A., Mountjoy, J.J., 2015. High-resolution seismic velocity analysis as a tool for exploring gas hydrate systems: An example from New Zealand's southern Hikurangi margin. *Interpretation* 4, SA1–SA12.
- De Rooij, M., Tingdahl, K., 2002. Meta-attributes—the key to multivolume, multiattribute interpretation. *Lead. Edge* 21(10), 1050–1053.
- Dewangan, P., Basavaiah, N., Badesab, F.K., Usapkar, A., Mazumdar, A., Joshi, R., Ramprasad, T., 2013. Diagenesis of magnetic minerals in a gas hydrate/cold seep environment off the Krishna-Godavari basin, Bay of Bengal. *Mar. Geol.* 340, 57-70.
- Dewangan, P., Mandal, R., Jaiswal, P., Ramprasad, T., Sriram, G., 2014. Estimation of seismic attenuation of gas hydrate bearing sediments from multi-channel seismic data: A case study from Krishna-Godavari offshore basin. *Mar. Pet. Geol.* 58, 356–367.
- Dewangan, P., Ramprasad, T., Ramana, M. V, Mazumdar, A., Desa, M., Badesab, F.K., 2010. Seabed morphology and gas venting features in the continental slope region of Krishna-Godavari basin, Bay of Bengal: Implications in gas-hydrate exploration. *Mar. Pet. Geol.* 27, 1628–1641.
- Dewangan, P., Sriram, G., Ramprasad, T., Ramana, M.V., Jaiswal, P., 2011. Fault system and thermal regime in the vicinity of site NGHP-01-10, Krishna-Godavari basin, Bay of Bengal. *Mar. Pet. Geol.* 28(10), 1899-1914.
- Dix, C.H., 1955. Seismic velocities from surface measurements. *Geophys.* 20, 68–86.

- Gullapalli, S., Dewangan, P., Kumar, A., Dakara, G., Mishra, C.K., 2019. Seismic evidence of free gas migration through the gas hydrate stability zone (GHSZ) and active methane seep in Krishna-Godavari offshore basin. *Mar. Pet. Geol.* 110, 695–705.
- Helgerud, M.B., Dvorkin, J., Nur, A., Sakai, A., Collett, T., 1999. Elastic-wave velocity in marine sediments with gas hydrates: Effective medium modeling. *Geophys. Res. Lett.* 26, 2021–2024.
- Hovland, M., Gallagher, J.W., Clennell, M.B., Lekvam, K., 1997. Gas hydrate and free gas volumes in marine sediments: Example from the Niger Delta front. *Mar. Pet. Geol.* 14, 245–255.
- Jaiswal, P., Dewangan, P., Ramprasad, T., Zelt, C.A., 2012a. Seismic characterization of hydrates in faulted, fine-grained sediments of Krishna-Godavari basin: Unified imaging. *J. Geophys. Res. Solid Earth* 117, B04306.
- Jaiswal, P., Dewangan, P., Ramprasad, T., Zelt, C.A., 2012b. Seismic characterization of hydrates in faulted, fine-grained sediments of Krishna-Godavari Basin: Full waveform inversion. *J. Geophys. Res. Solid Earth* 117, B10305.
- Kinoshita, M., Moore, G.F., Kido, Y.N., 2011. Heat flow estimated from BSR and IODP borehole data: Implication of recent uplift and erosion of the imbricate thrust zone in the Nankai Trough off Kumano. *Geochemistry, Geophys. Geosystems* 12(9), doi:10.1029/2011GC003609.
- Krishna, K.S., Ismaiel, M., Srinivas, K., Gopala Rao, D., Mishra, J., Saha, D., 2016. Sediment pathways and emergence of Himalayan source material in the Bay of Bengal. *Curr. Sci.* 110, 363–372.
- Kumar, P., Collett, T.S., Boswell, R., Cochran, J.R., Lall, M., Mazumdar, A., Ramana, M.V., Ramprasad, T., Riedel, M., Sain, K., Sathe, A.V., Vishwanath, K., Yadav, U.S., 2014. Geologic implications of gas hydrates in the offshore of India: Krishna–Godavari Basin, Mahanadi Basin, Andaman Sea, Kerala–Konkan Basin. *Mar. Pet. Geol.* 58, 29–98.
- Kundu, N., Pal, N., Sinha, N., Budhiraja, I.L., 2008. Paleo hydrate and its role in deep water Plio-Pleistocene gas reservoirs in Krishna-Godavari Basin, India. In: 6th International Conference on Gas Hydrates (ICGH2008), Vancouver 2008.
- Kvenvolden, K.A., 2002. Methane hydrate in the global organic carbon cycle. *Terra Nov.* 14, 302–306.
- Kvenvolden, K.A., 1993. Gas hydrates-geological perspective and global change. *Rev. Geophys.* 31, 173–187.
- Kvenvolden, K.A., 1988. Methane hydrate - a major reservoir of carbon in the shallow geosphere? *Chem. Geol.* 71, 41–51.
- Liu, X., Flemings, P.B., 2007. Dynamic multiphase flow model of hydrate formation in marine sediments. *J. Geophys. Res. Solid Earth* 112, B03101.
- Mandal, R., Dewangan, P., Ramprasad, T., Kumar, B.J.P., Vishwanath, K., 2014. Effect of thermal non-equilibrium, seafloor topography and fluid advection on BSR-derived geothermal gradient. *Mar. Pet. Geol.* 58, 368–381.

- Mazumdar, A., Dewangan, P., João, H.M., Peketi, A., Khosla, V.R., Kocherla, M., Badesab, F.K., Joshi, R.K., Roxanne, P., Ramamurty, P.B., Karisiddaiah, S.M., Patil, D.J., Dayal, A.M., Ramprasad, T., Hawkesworth, C.J., Avanzinelli, R., 2009. Evidence of paleo-cold seep activity from the Bay of Bengal, offshore India. *Geochemistry, Geophys. Geosystems* 10 (6), 15. doi:10.1029/2008GC002337
- Mazumdar, A., Dewangan, P., Peketi, A., Gullapalli, S., Kalpana, M.S., Naik, G.P., Shetty, D., Pujari, S., Pillutla, S.P.K., Gaikwad, V. V, Nazareth, D., Sangodkar, N.S., Dakara, G., Kumar, A., Mishra, C.K., Singha, P., Reddy, R., 2019. The first record of active methane (cold) seep ecosystem associated with shallow methane hydrate from the Indian EEZ. *J. Earth Syst. Sci.* 128, 18.
- Milkov, A. V, Sassen, R., 2002. Economic geology of offshore gas hydrate accumulations and provinces. *Mar. Pet. Geol.* 19, 1–11.
- Milkov, A. V, Sassen, R., 2001. Estimate of gas hydrate resource, northwestern Gulf of Mexico continental slope. *Mar. Geol.* 179, 71–83.
- Minshull, T.A., Singh, S.C., Westbrook, G.K., 1994. Seismic velocity structure at a gas hydrate reflector, offshore western Colombia, from full waveform inversion. *J. Geophys. Res. Solid Earth* 99(B3), 4715-4734.
- Neidell, N.S., Taner, M.T., 1971. Semblance and other coherency measures for multichannel data. *Geophys.* 36, 482–497.
- Pecher, I. A., Henrys, S. A., Wood, W.T., Kukowski, N., Crutchley, G.J., Fohrmann, M., Kilner, J., Senger, K., Gorman, A.R., Coffin, R.B., Greinert, J., Faure, K., 2010. Focussed fluid flow on the Hikurangi Margin, New Zealand — Evidence from possible local upwarping of the base of gas hydrate stability. *Mar. Geol.* 272, 99–113.
- Powell C. M., Roots, S.R., Veevers, J.J., 1988. Pre-breakup continental extension in east Gondwanaland and the early opening of the eastern Indian Ocean. *Tectonophysics* 155, 261–283.
- Ramana, M. V, Nair, R.R., Sarma, K.V.L.N.S., Ramprasad, T., Krishna, K.S., V., S., D’Cruz, M., Subrahmanyam, C., Paul, J., Subrahmanyam, A.S., Sekhar, D.V.C., 1994. Mesozoic anomalies in the Bay of Bengal. *Earth Planet. Sci. Lett.* 121, 469–475.
- Ramprasad, T., Dewangan, P., Ramana, M.V., Mazumdar, A., Karisiddaiah, S.M., Ramya, E.R., Sriram, G., 2011. Evidence of slumping/sliding in Krishna-Godavari offshore basin due to gas/fluid movements. *Mar. Pet. Geol.* 28(10), 1808-1816.
- Rao, G.N., 2001. Sedimentation, stratigraphy, and petroleum potential of Krishna-Godavari basin, East Coast of India. *Am. Assoc. Pet. Geol. Bull.* 85(9), 1623-1643
- Rao, G.N., Mani, K.S., 1993. A study on generation of abnormal pressures in Krishna Godavari basin. *Indian J. Pet. Geol.* 2, 20–30.
- Riedel, M., Collett, T.S., Kumar, P., Sathe, A. V., Cook, A., 2010. Seismic imaging of a fractured gas hydrate system in the Krishna–Godavari Basin offshore India. *Mar. Pet. Geol.* 27, 1476–1493.

- Sassen, R., Losh, S.L., Cathles III, L., Roberts, H.H., Whelan, J.K., Milkov, A. V, Sweet, S.T., DeFreitas, D.A., 2001. Massive vein-filling gas hydrate: relation to ongoing gas migration from the deep subsurface in the Gulf of Mexico. *Mar. Pet. Geol.* 18(5), 551–560.
- Sava, P., Biondi, B., 2004. Wave-equation migration velocity analysis. I. Theory. *Geophys. Prospect.* 52, 593–606.
- Schmuck, E.A., Paull, C.K., 1993. Evidence for gas accumulation associated with diapirism and gas hydrates at the head of the Cape Fear Slide. *Geo-Marine Lett.* 13, 145–152.
- Scotese, C.R., Gahagan, L.M., Larson, R.L., 1988. Plate tectonic reconstructions of the Cretaceous and Cenozoic ocean basins. *Tectonophysics* 155, 27–48.
- Sheriff, R. E., 1980. Nomogram for Fresnel-zone calculation. *Geophysics* 45, 968–972.
- Singh, S.C., Minshull, T.A., Spence, G.D., 1993. Velocity structure of a gas hydrate reflector. *Science.* 260, 204–207.
- Singha, D.K., Chatterjee, R., 2014. Detection of overpressure zones and a statistical model for pore pressure estimation from well logs in the Krishna-Godavari Basin, India. *Geochemistry, Geophys. Geosystems* 15, 1009–1020.
- Sloan, E.D., Koh, C., 2007. *Clathrate hydrates of natural gases.* CRC Press.
- Sriram, G., Dewangan, P., Ramprasad, T., Rama Rao, P., 2013. Anisotropic amplitude variation of the bottom-simulating reflector beneath fracture-filled gas hydrate deposit. *J. Geophys. Res. Solid Earth* 118, 2258–2274.
- Sriram, G., Dewangan, P., Ramprasad, T., 2014. Modified effective medium model for gas hydrate bearing, clay-dominated sediments in the Krishna–Godavari Basin. , *Mar. Pet. Geol.* 58, 321–330.
- Stork, C., 1992. Reflection tomography in the postmigrated domain. *Geophysics* 57, 680–692.
- Stranne, C., O’Regan, M., Jakobsson, M., 2017. Modeling fracture propagation and seafloor gas release during seafloor warming-induced hydrate dissociation. *Geophys. Res. Lett.* 44, 8510–8519.
- Suess, E., Torres, M.E., Bohrmann, G., Collier, R.W., Rickert, D., Goldfinger, C., Linke, P., Heuser, A., Sahling, H., Heeschen, K., Jung, C, 2001. Sea floor methane hydrates at Hydrate Ridge, Cascadia margin. *Geophys. Monogr.* 124, 87–98.
- Taladay, K., Boston, B., Moore, G. , 2017. Gas-in-place estimate for potential gas hydrate concentrated zone in the Kumano Basin, Nankai Trough Forearc, Japan. *Energies*, 10(10), 1552.
- Toldi, J., 1989. One-Dimensional Velocity Analysis Without Picking. *Geophys.* 54, 191–199.
- Torres, M.E., Wallmann, K., Tréhu, A. M., Bohrmann, G., Borowski, W.S., Tomaru, H., 2004. Gas hydrate growth, methane transport, and chloride enrichment at the southern summit of Hydrate Ridge, Cascadia margin off Oregon. *Earth Planet. Sci. Lett.* 226, 225–241.

- Usapkar, A., Dewangan, P., Kocherla, M., Ramprasad, T., Mazumdar, A., Ramana, M. V, 2014. Enhanced methane flux event and sediment dispersal pattern in the Krishna-Godavari offshore basin: Evidences from rock magnetic techniques. *Mar. Pet. Geol.* 58, 461–475.
- Van Tuyl, J., Alves, T. M., Moore, G. F. , 2015. Strain decoupling reveals variable seismogenic risk in SE Japan (Nankai Trough). *Geochemistry, Geophys, Geosystems*, 16(7), 2025-2037.
- Yilmaz, Ö., 2001. *Seismic data analysis: Processing, inversion, and interpretation of seismic data.* Society of exploration geophysicists.

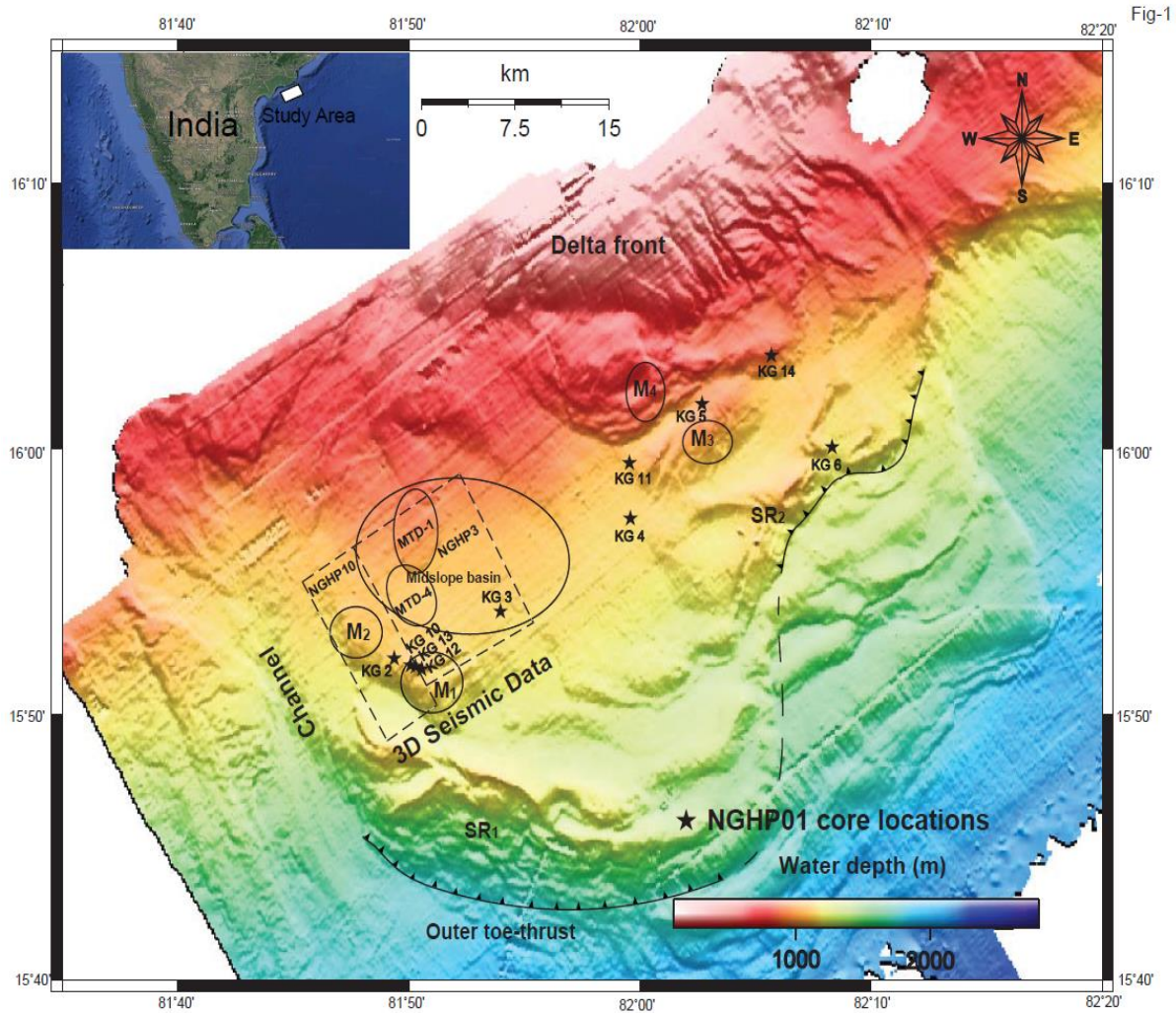


**Fig. 1**



Fig.2

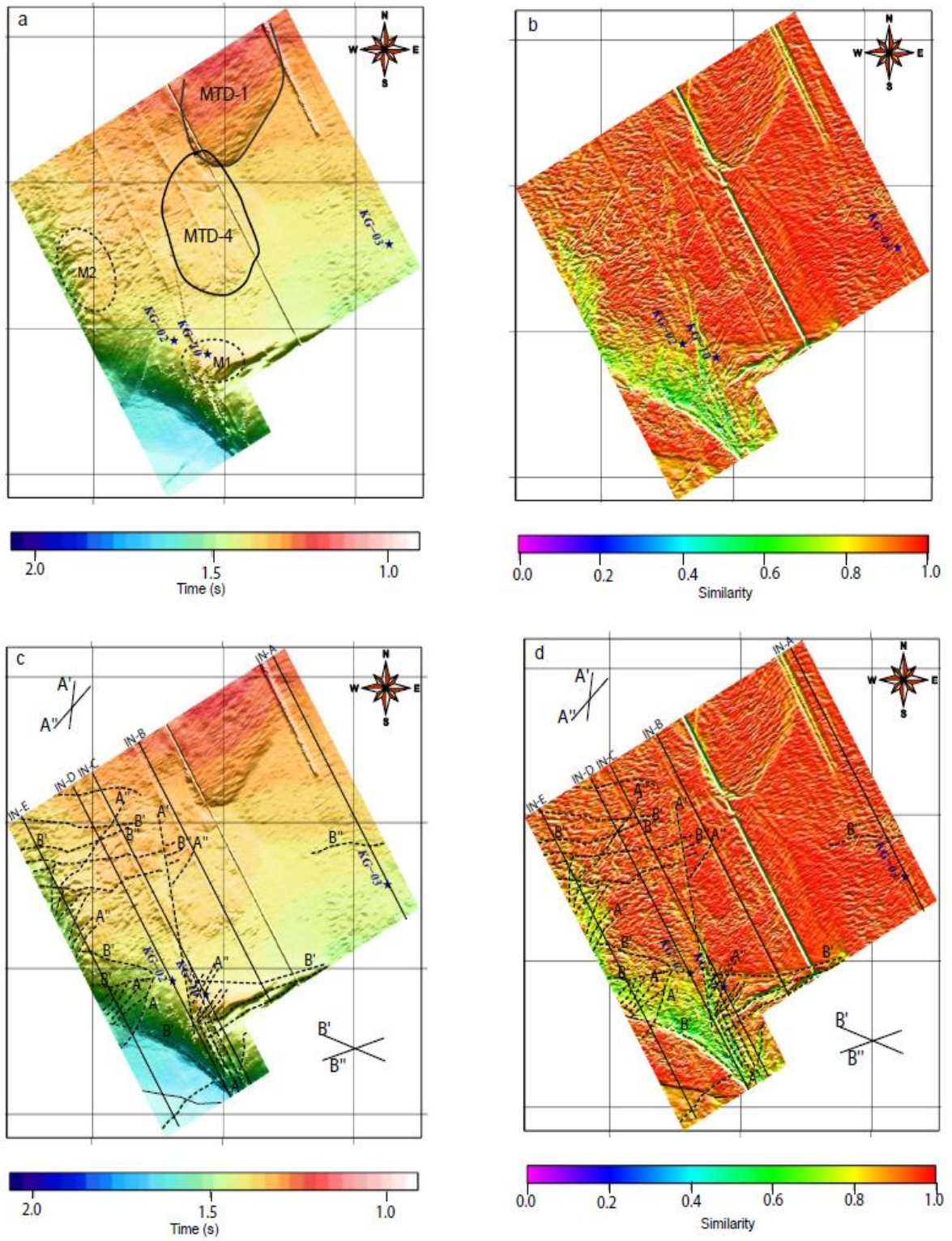


Fig. 2

Fig. 3a

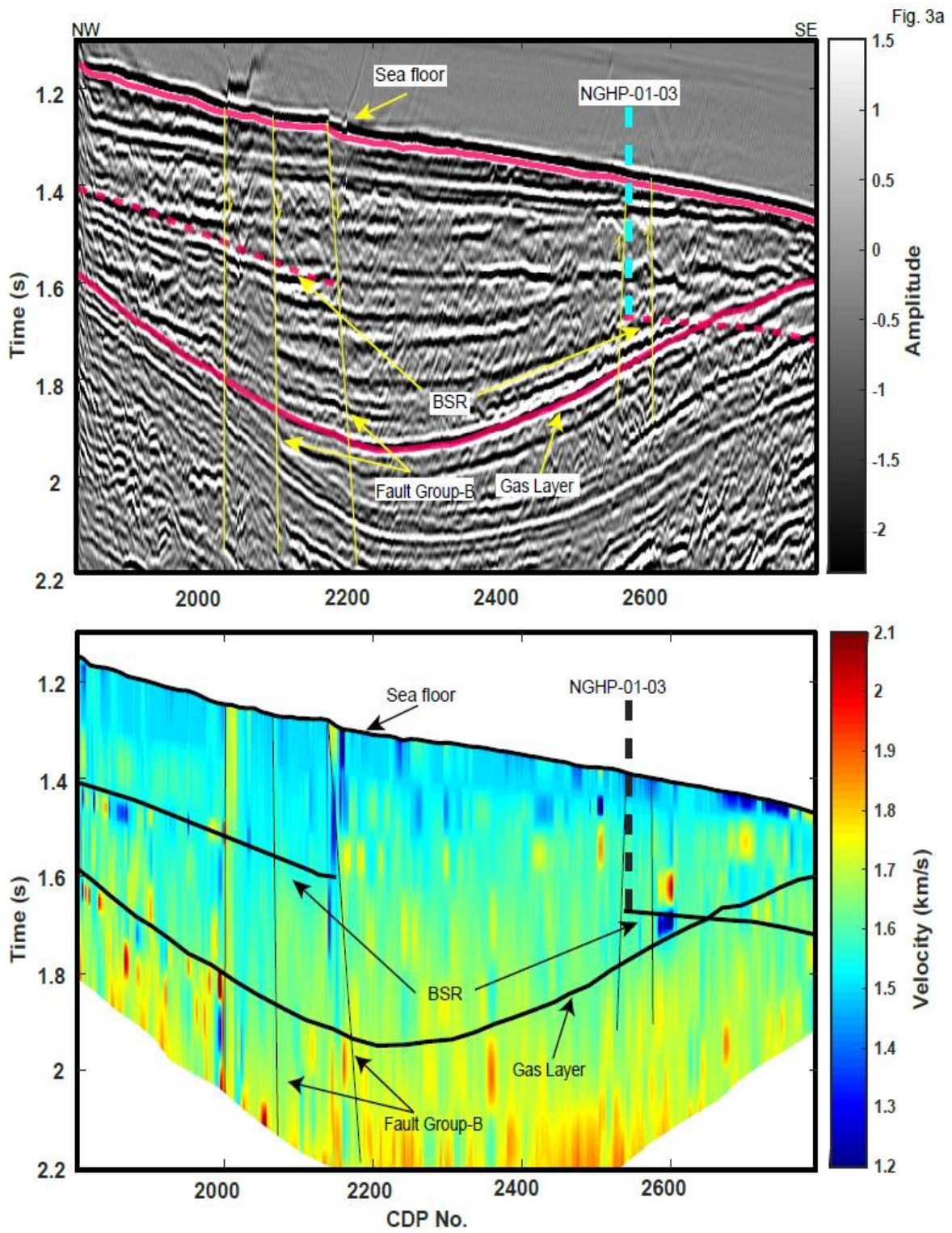




Fig. 3b

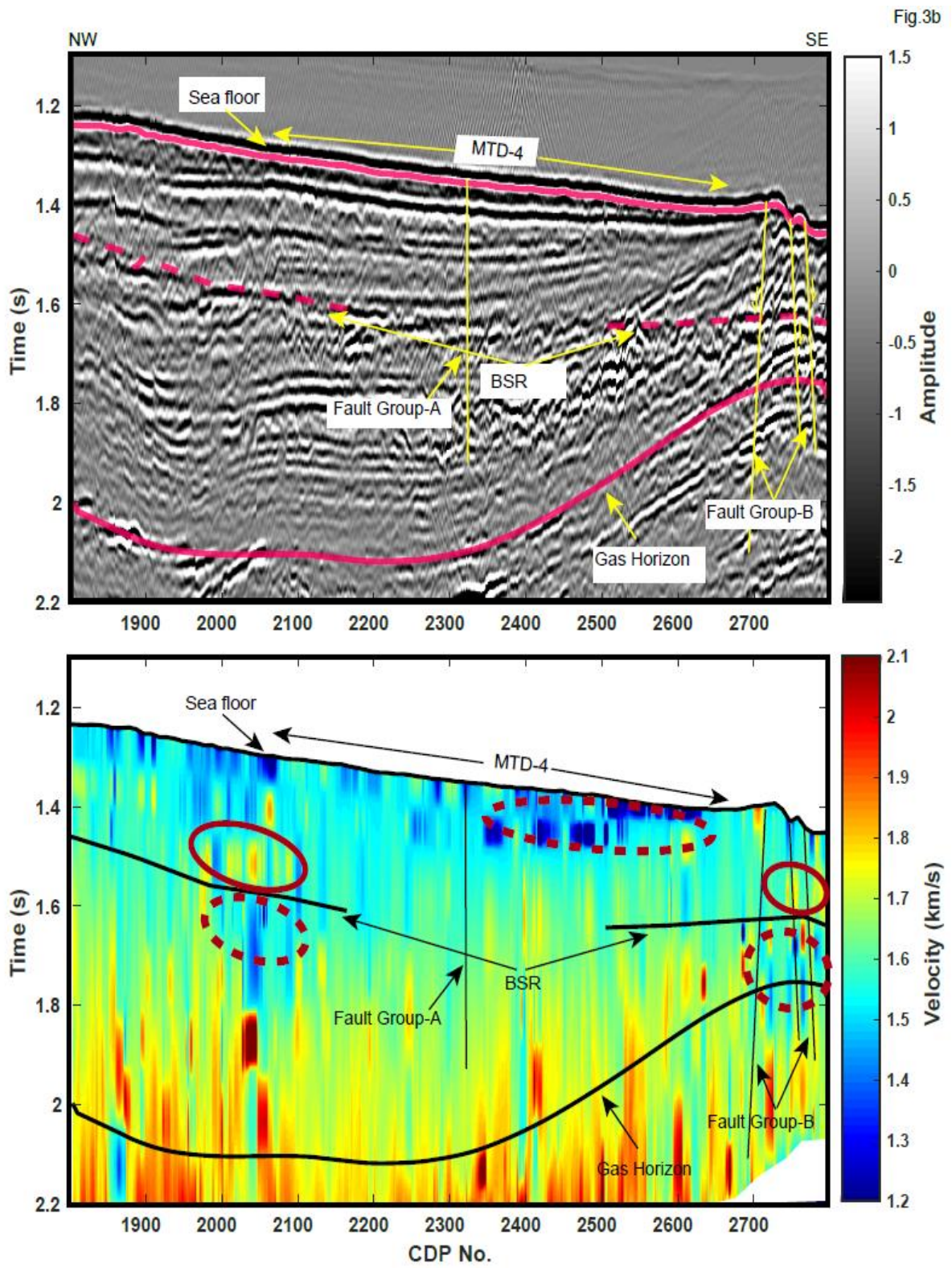


Fig. 3c

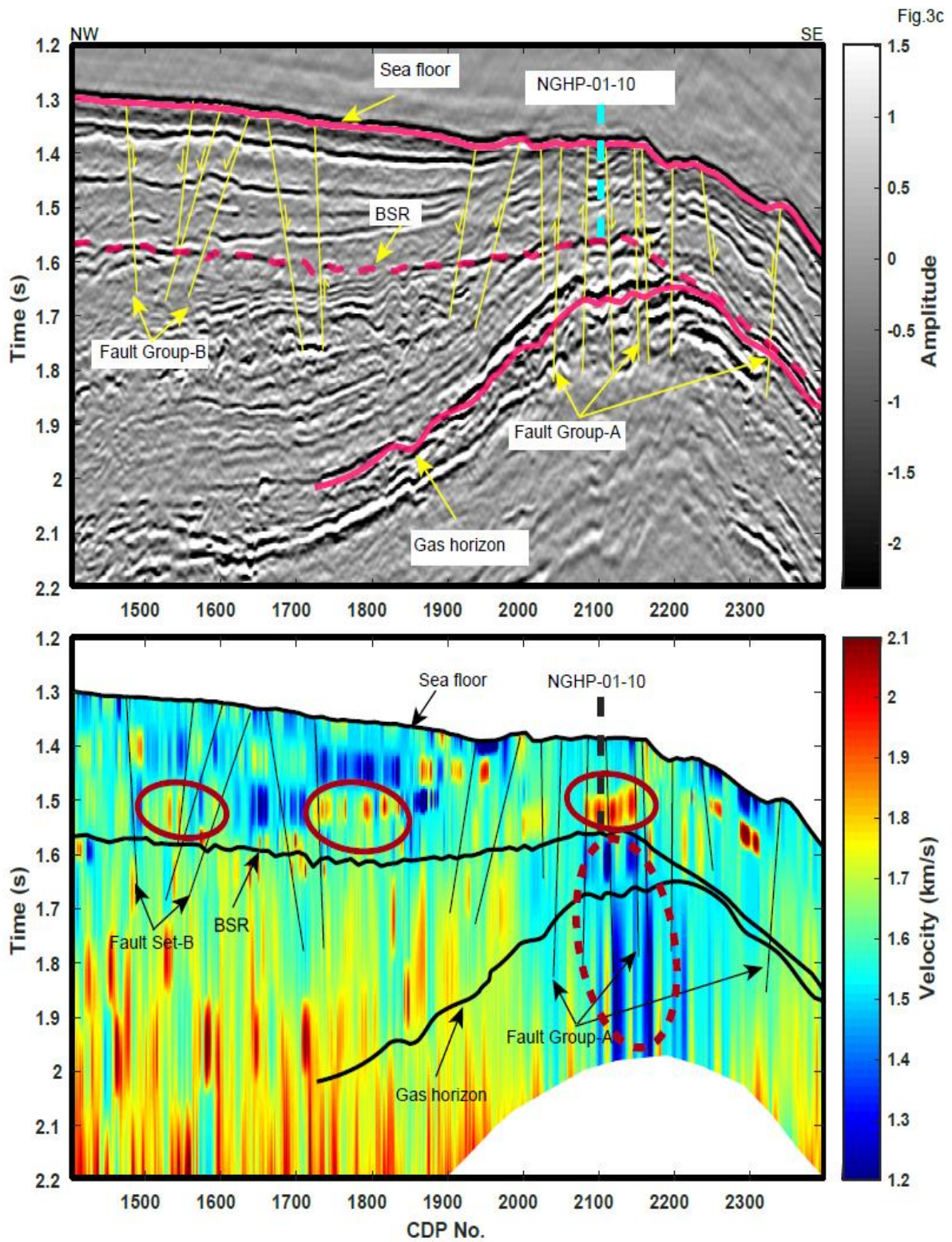




Fig. 3d

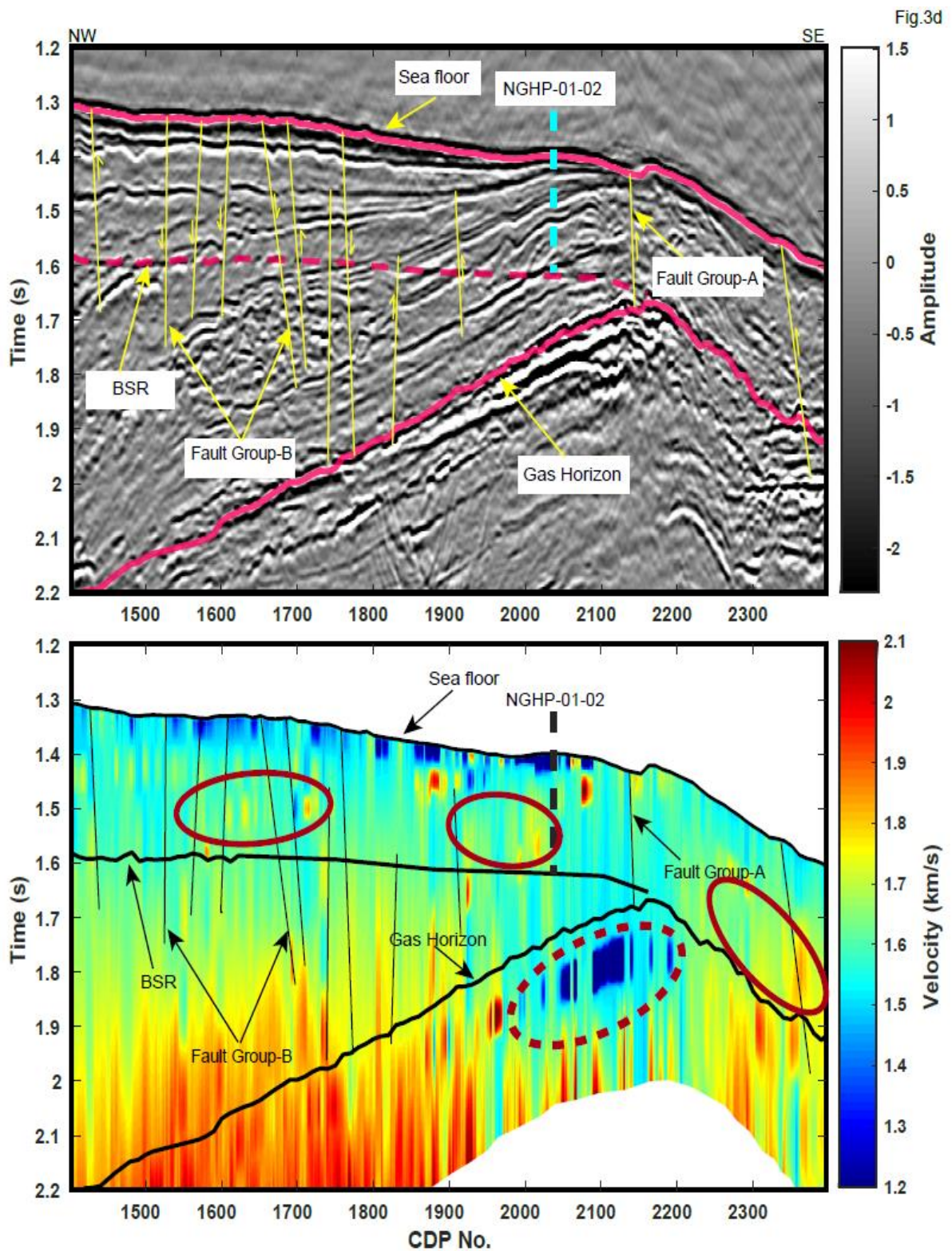


Fig. 3e

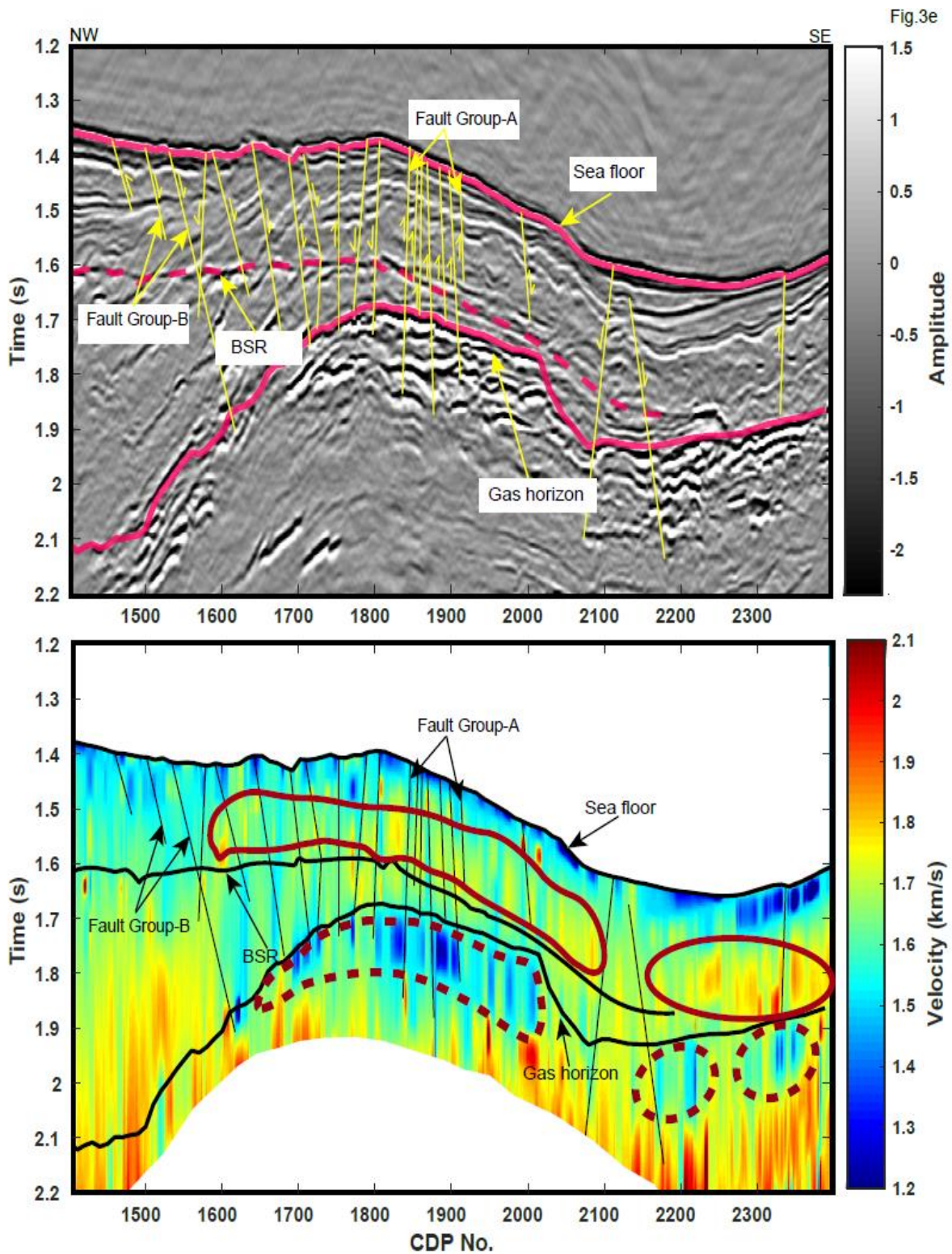
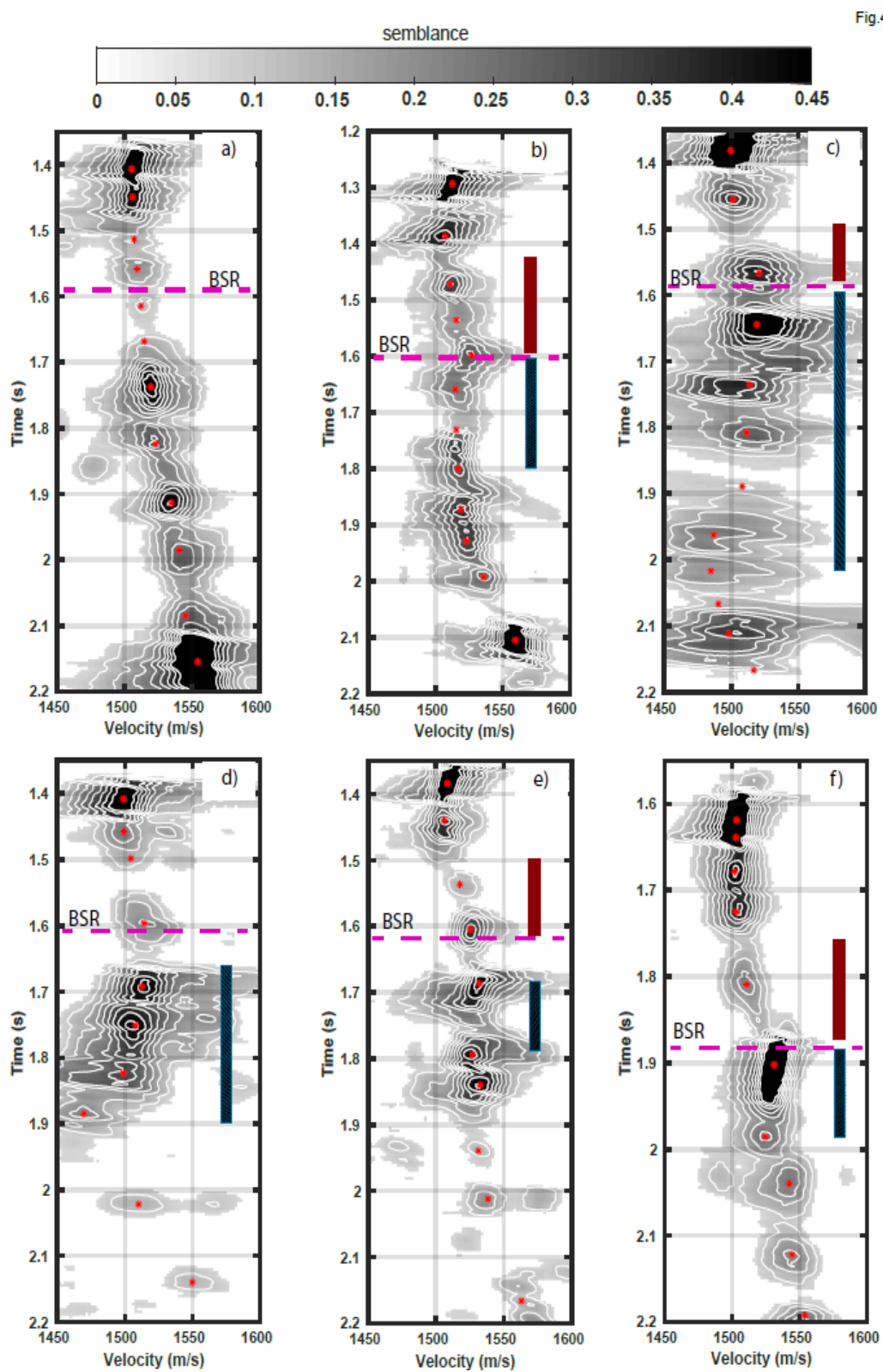




Fig. 4



**Fig. 5**

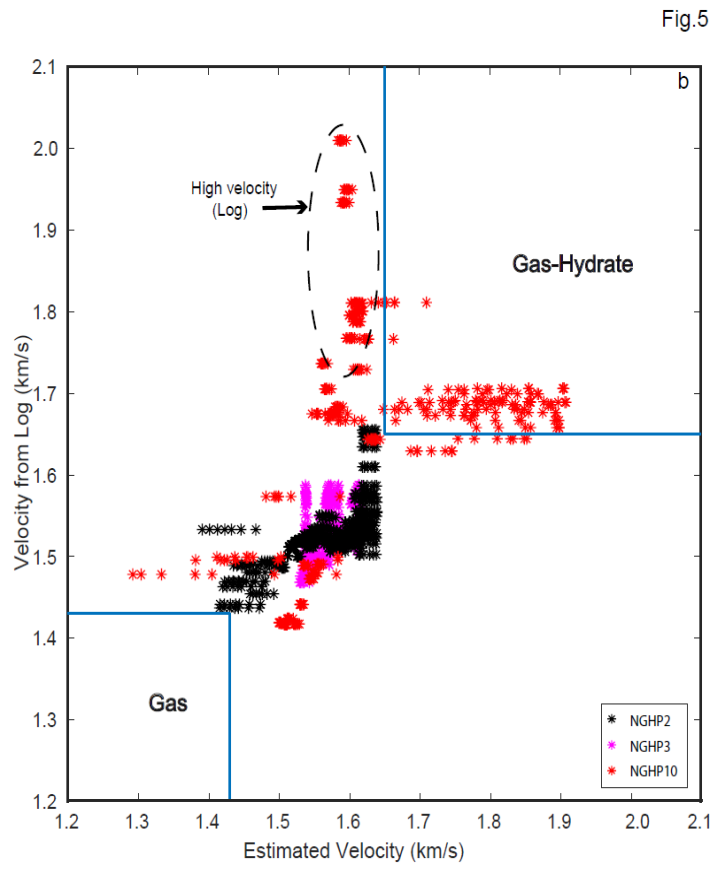
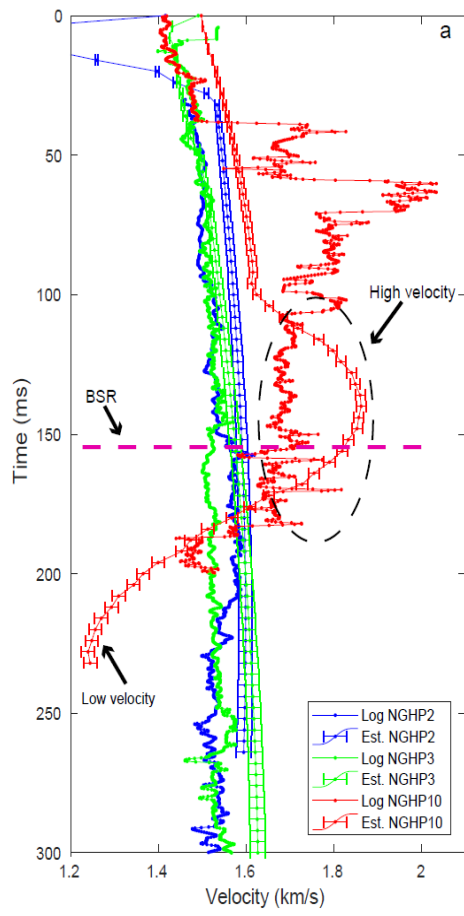


Fig. 6

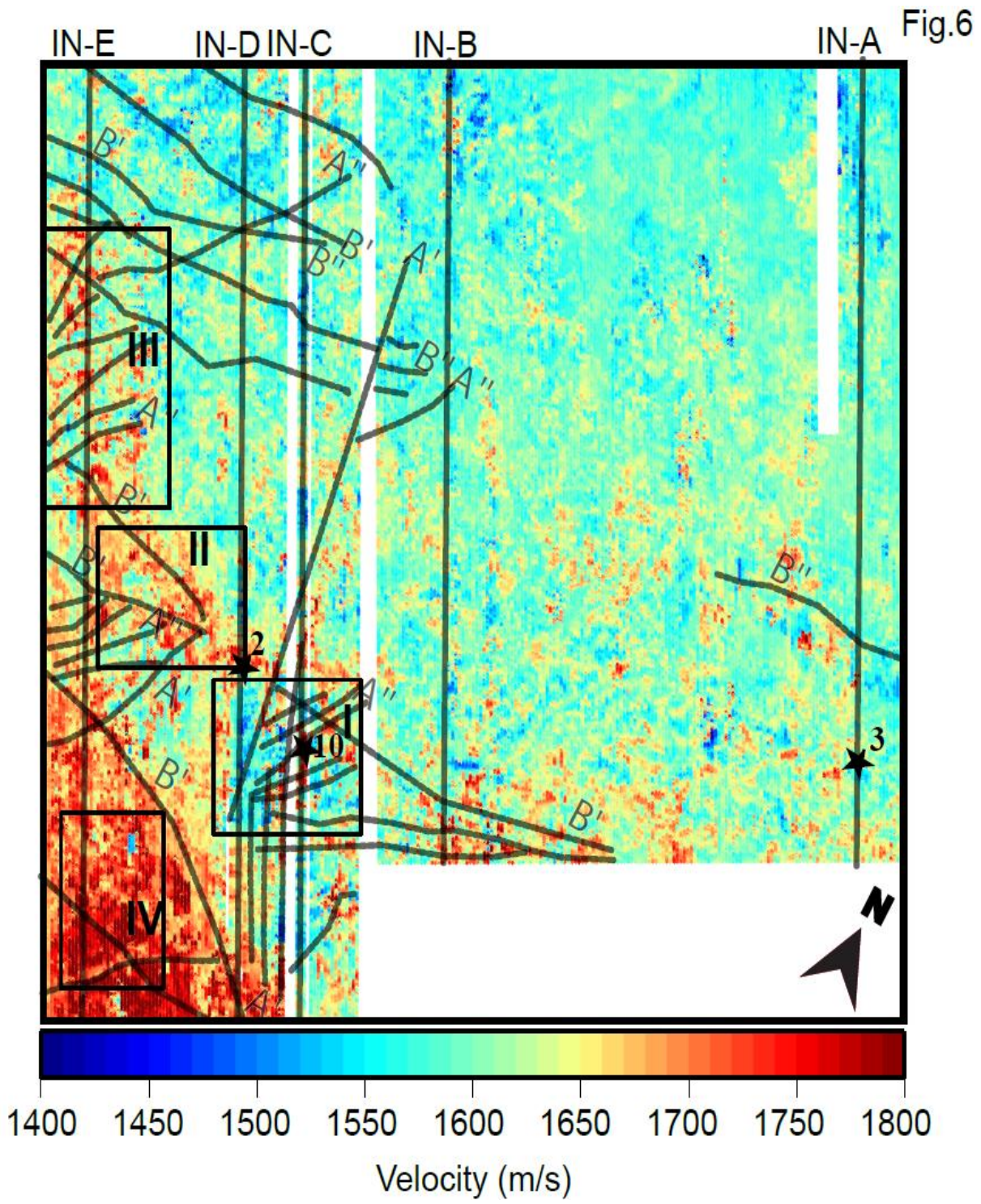




Fig. 7

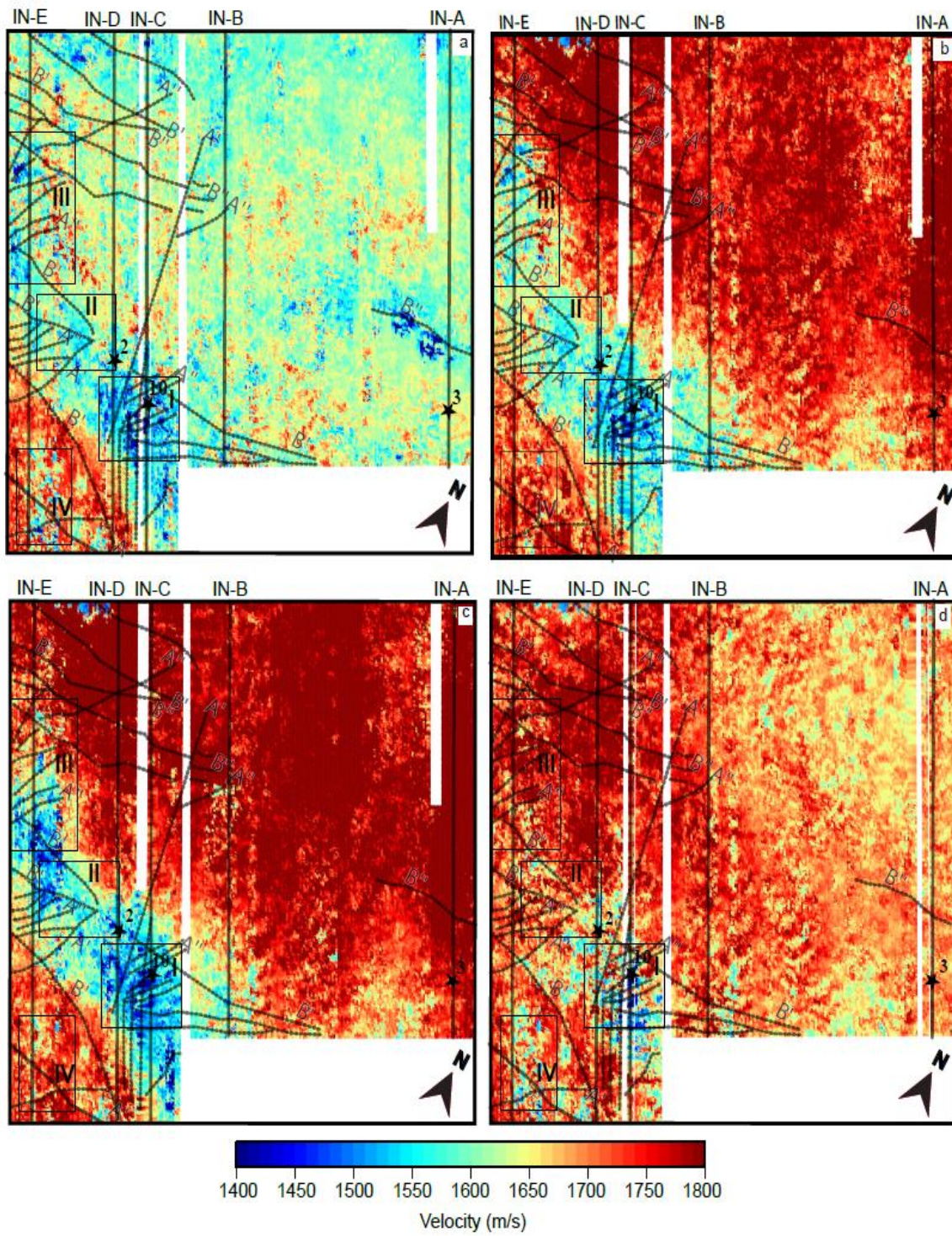
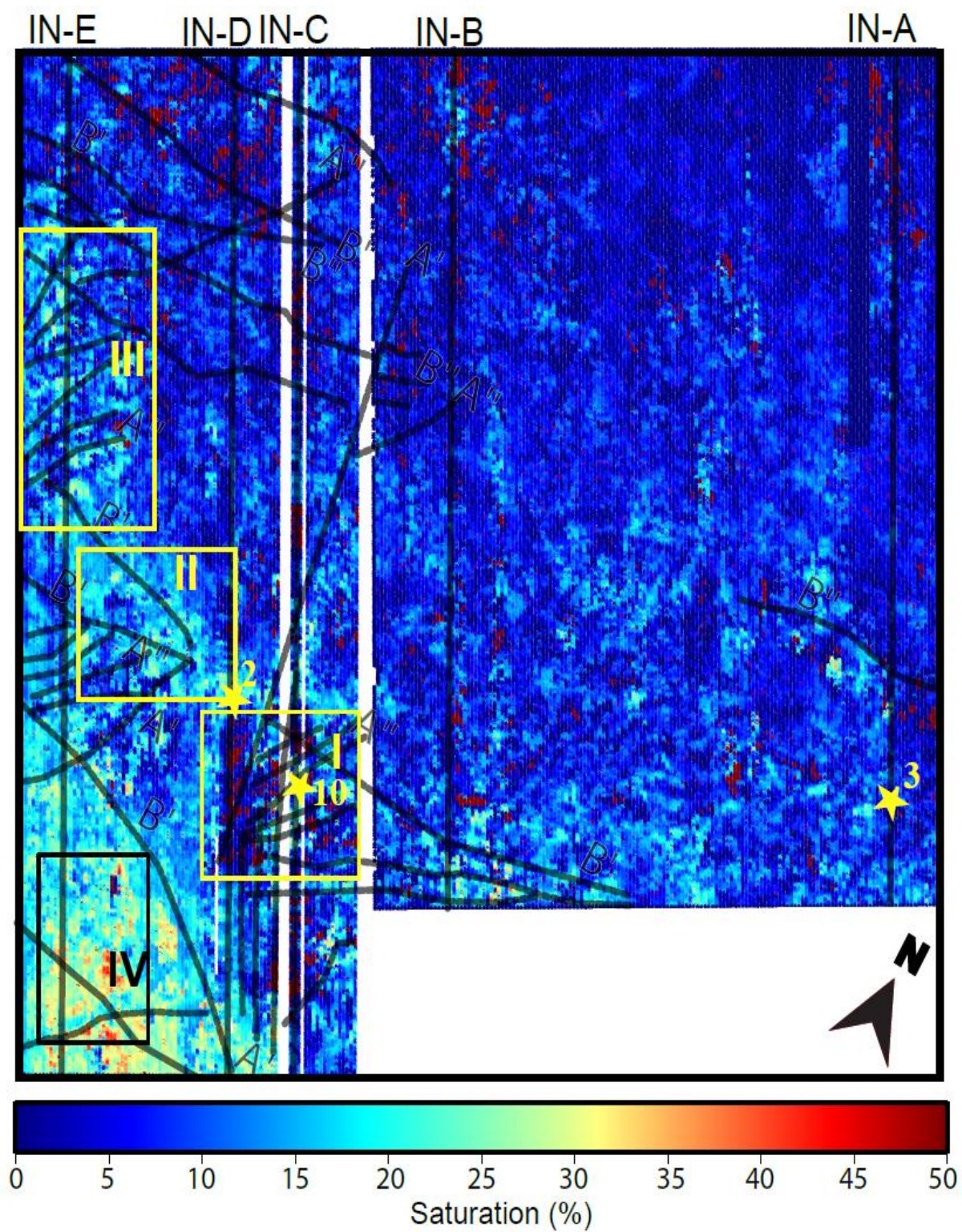




Fig. 8



**Fig. 9**

